Heavy residue production in the interaction of 29 MeV/nucleon ^{208}Pb with ^{197}Au

W. Loveland,[1] M. Andersson,[1] K. E. Zyromski,[1] N. Ham,[1] B. Altschul,[1] J. Vlcakova,[1] D. Menge,[1] J. O. Liljenzin,[2] R. Yanez,[3] and K. Aleklett[3]

[1]*Department of Chemistry, Oregon State University, Corvallis, Oregon 97331*

[2]*Chalmers University of Technology, Göteborg, Sweden*

[3]*Studsvik Neutron Research Laboratory, S-611 82 Nyköping, Sweden*

(Received 5 October 1998)

The yields, recoil properties, and angular distributions of the fragments of the target nucleus were measured for the 29 MeV/nucleon ^{208}Pb+^{197}Au reaction using radiochemical techniques. The fragment isobaric yield distribution and mean energies were deduced from these data. The fission cross section is 2.2 ± 0.5 b while the residue formation cross section is 3.9 b. Heavy residues form a part of a large central bump (usually associated with fission) in the fragment mass distribution. Comparing the data from this reaction to other reactions involving massive nuclei at projectile energies from 7 to 45 MeV/nucleon shows the locus of fragment yields $[\sigma(Z,A)]$ to be roughly independent of the reacting system or projectile energy. The fragment angular distributions evolve from sidewise peaked (for near target, quasielastic residues) to forward peaked as the mass number decreases. The isomer ratios for the residues indicate their formation from the lowest partial wave events while the fission fragments appear to originate in higher l events. Attempts to use the nucleon transport model (or some modification of it) to calculate the residue cross sections were only partially successful. It is suggested the the lack of dynamic multifragmentation mechanisms in these models is the cause of the shortcomings. [S0556-2813(99)01203-0]

PACS number(s): 25.70.Mn, 25.70.Jj, 25.70.Lm

I. INTRODUCTION

In the study of intermediate energy nuclear collisions, much attention has been given to understanding the reaction mechanisms involved. One theme has been to relate the observed phenomena to some appropriate modification of the familiar low energy reaction mechanisms (such as complete/incomplete fusion, deep inelastic scattering, etc.) or high energy mechanisms (such as projectile fragmentation). The collision of massive nuclei, such as Xe + Au, Bi or Pb + Au, has proven to be especially interesting. Because of the large Coulomb forces present in the interaction, fusion or fusion-like phenomena are not expected [1]. Dissipative phenomena might be expected to be very important if our experience with low energy collisions between massive nuclei can be extrapolated to this energy regime. The postinteraction phenomena in these collisions are complicated, with possibilities of pre-equilibrium emission, pre- and postscission evaporation, fission, intermediate mass fragment (IMF) emission or multifragmentation of both reacting nuclei. These phenomena make studies of these collisions challenging.

One reaction, the reaction of 29 MeV/nucleon ^{208}Pb with ^{197}Au, has been extensively studied [2–13] as part of the effort to understand the collisions between these massive nuclei. Based upon these studies (and complementary studies [14–18] of the 27-28 MeV/nucleon Xe+^{197}Au, ^{209}Bi reactions) one concludes the following.

The dominant reaction mechanism involves a binary dissipative primary collision [3,5–7,11,14–16].

Surviving residues of the primary projectilelike fragment (PLF) result from the lowest multiplicity events that can be understood in terms of nucleon exchange models [19] used to describe low energy deep inelastic scattering [2,6].

PLFs that fission result from peripheral collisions with greater associated multiplicities than events leading to residue formation, but result in excitation energies E^* >300 MeV. The angular momentum transfer in these collisions is $>40\hbar$ with highly aligned spins. The fissioning PLFs are the high Z members of the primary PLF distributions [4,6].

Preequilibrium emission of nucleons is small [3,6].

Highly excited ($T\sim7$ MeV) nuclei are produced in binary events involving large dissipation (up to ~2.4 GeV), resulting in IMF emission [2,5–7,9–11].

The studies that lead to these conclusions, while involving detection of the emitted PLFs, neutrons, fission fragments, IMFs, and charged particles, had a limited acceptance for the expected low energy primary residues of the target nucleus. These studies and the conclusions themselves, however, give obvious predictions for the properties of the target-like-fragments (TLFs) produced in the 29 MeV/nucleon ^{208}Pb + ^{197}Au reaction. We thought that we could provide additional information about the Pb+Au reaction (the properties of the TLFs) along with testing the ideas outlined above by making a radiochemical study of the properties of the TLFs formed in this reaction. The use of radiochemical techniques to measure the TLF properties should give a threshold-free measurement with superior Z and A resolution that is difficult, if not impossible, to achieve using physical techniques [20].

II. EXPERIMENTAL

These radiochemical experiments were performed at the GANIL laboratory (Grand Acclerateur National d'Ions Lourds) at Caen, France. The experimental techniques used have been described previously [21]. Three separate irradiations were performed. In the first experiment, a

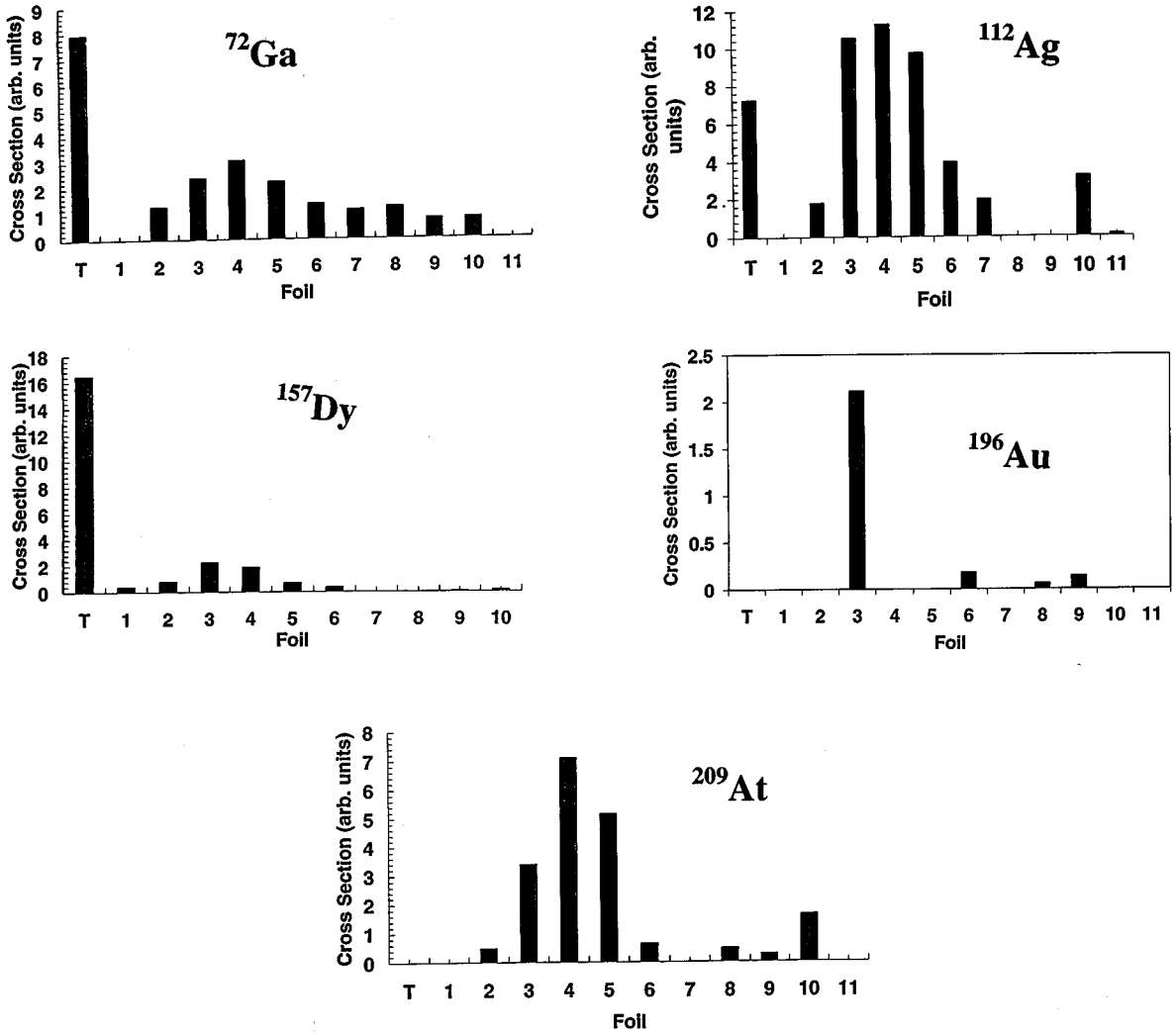

FIG. 1. Representative range spectra (7–45°) for the 29 MeV/nucleon ^{208}Pb+^{197}Au reaction, showing the separation between PLF and TLF components. T represents the target foil while the other foils in order of depth in the stack are represented by the foil number.

24.3 mg/cm^2 ^{197}Au target was irradiated with a beam of 29 MeV/nucleon ^{208}Pb ions. Projectilelike fragments (PLFs) and targetlike fragments (TLFs) emerging at angles of 7–45° were stopped in a stack of 10 mg/cm^2 C foils (11 foils). This apparatus was irradiated for 158 min with an average flux of 1.73×10^{11} ions/min. In the second irradiation, a 24.1 mg/cm^2 ^{197}Au target was irradiated with a flux of 1.88×10^{11} ions/min for 174 min. Fragments recoiling forward or backward from the thick Au target were stopped in a 10.7 mg/cm^2 C foil. In the third irradiation, a thin 300 μ g/cm^2 ^{197}Au target was irradiated for 1460 min with an average flux of 7.7×10^{10} ions/min. The thin Au target was at the center of an evacuated cylindrical scattering chamber lined with 17.4 mg/cm^2 Mylar. The TLFs emerging from the Au target were stopped in the Mylar, which was cut up after irradiation to correspond to the desired angular intervals. These three irradiations will be referred to as the ''PLF-range,'' the ''thick target-thick catcher'' and the ''angular distribution'' experiments. The center-of-target beam energies were 27.0, 26.9, and 29.0 MeV/nucleon [22]. To facilitate comparison with previous work and because the differences in projectile energy are not thought to be significant, we shall refer to the incident projectile energy, 29 MeV/nucleon, in describing our measurements. The radionuclide content of the targets and catcher foils was determined by off-line γ-ray spectroscopy that was carried out at GANIL, Oregon State University, and the Chalmers University of Technology for a period ranging from a few minutes after the end of bombardment to several months. Production cross sections were calculated from end-of-bombardment activities [21]. Typically we observed 2–3 γ-rays per nuclide with the range being 1–10.

III. RESULTS

In a radiochemical experiment in which the projectile and target nuclei are of comparable size, one must distinguish between fragments originating in the target or projectile nuclei. In the ''PLF-range'' experiment, the range (energy) distributions of the PLFs and TLFs emerging at angles of 7–45° were measured for 228 different radionuclides (Fig. 1). For each of these radionuclides, it was possible to separate the observed distributions into a PLF and a TLF component based upon their energies (Fig. 1). Based upon this

separation of the fragments by range (energy), we concluded that, apart from small correction factors (generally $\leqslant 10\%$), the nuclides that stopped in the target foil and the first (~ 10 mg/cm^2 carbon) catcher foil were targetlike fragments. (Similarly the TLFs did not, in general, penetrate to the second catcher foil of the ten foil stack.) Based upon this measurement, we conclude that, apart from small correction factors, the ''thick target-thick catcher'' experiment only sampled TLFs. [The PLFs generally punched through the forward (10.7 mg/cm^2 carbon) catcher foil.]

The nuclidic production cross sections as determined in the thick target-thick catcher experiment for 102 different TLFs formed in the interaction of 29 MeV/nucleon ^{208}Pb with ^{197}Au are listed in Table I. Also shown in these tables are the thick target-thick catcher recoil properties F/B and 2W(F+B). F/B is the ratio of the products recoiling into the forward (F) and backward (B) catcher foils while 2W(F+B) represents the fraction of all nuclides recoiling out of the target, F+B, multiplied by twice the target thickness, W. F/B is a range-weighted measure of the fragment angular distributions, while 2W(F+B) is proportional to the fragment range (energy).

To more fully utilize the cross section data shown in Table I, we have deduced mass-yield (isobaric yield) distributions from the measured formation cross sections. The method employed in this estimation procedure has been discussed previously [25].

The measured nuclidic formation cross sections were placed in eleven groups according to mass number. These cross sections were corrected for precursor beta or alpha decay, where necessary, by assuming that the independent yield cross sections for a given species, $\sigma(Z,A)$, can be expressed as a function of the isobaric yield $\sigma(A)$ as

$$\sigma(Z,A)=0.5\sigma(A)[\mathrm{erf}(u)-\mathrm{erf}(w)], \tag{1}$$

where

$$u=(Z-Z_{\mathrm{mp}}+0.5)/C_z(A)\sqrt{2} \tag{2}$$

and

$$w=(Z-Z_{\mathrm{mp}}-0.5)/C_z(A)\sqrt{2}. \tag{3}$$

Here $C_z(A)$ is the Gaussian width parameter for mass number A, $\mathrm{erf}(x)$ is the error function of x, and $Z_{\mathrm{mp}}(A)$ is the most probable atomic number for that A. Using this assumption and the further assumption that $\sigma(A)$ varies slowly and smoothly as a function of A [allowing data from adjacent isobars to be combined in determining $Z_{\mathrm{mp}}(A)$ and $C_z(A)$], one can use the laws of radioactive decay to iteratively correct the measured cumulative formation cross sections for precursor decay.

Within each group, the data were fitted by a Gaussian-shaped independent yield distribution. (Only nuclides with well-characterized beta- or alpha-decay precursors and well-understood members of an isomeric pair were included in the analysis.) The nuclide groupings along with the centers and widths of the Gaussian distributions are given in Table II and Fig. 2. The independent yield distributions deduced from the measured formation cross sections are shown in Fig. 3. The deduced values of Z_{mp}/A are uncertain to 0.005 unit while those of C_z are typically uncertain to 0.1 Z unit.

While the Z_{mp} values deduced from this analysis are expected to have large uncertainties, it may be instructive to compare the values deduced from our analysis with values deduced from other studies of N/Z equilibration in massive collisions. As shown in Fig. 2, the Z_{mp} values for the fragmentation of ^{197}Au by 21 MeV/nucleon ^{129}Xe [28] and 29 MeV/nucleon ^{208}Pb are virtually identical (except for the lightest products) as are those observed in Xe-Au collisions at 6.8 MeV/nucleon [29].

We note further (Fig. 2) that these Z_p values are not those associated with the line of β stability, i.e., the mass surface is not determining the position of Z_p. Furthermore we note (Fig. 2) that the locus of Z_p is not that seen in relativistic nuclear collisions [23], nor are the Z_p values as large as those seen in relativistic nuclear collisions, i.e., these nuclei are not as neutron deficient as those resulting from higher energy collisions. Comparison with models for these collisions (see below) indicates the primary distributions in the two reactions are not very similar and so any similarity in the secondary product distributions is surprising.

We can pursue this point further by comparing (Fig. 4) the deduced Z_p functions for a wide variety of reactions [28,30] involving massive nuclei. The measured Z_p functions for these reactions spanning projectile ranges from 6.8 to 45 MeV/nucleon and involving both Xe and Pb projectiles appear to be very similar apart from the differences for the lightest products (IMFs). It appears that the evaporation of neutrons and charged particles from differing assortments of excited primary reaction products leads to a common locus in the N-Z plane of the product nuclei. This locus has been referred to as the ''evaporation residue attractor'' line [24] although the observed line in this work differs from statistical model predictions [28]. For the case of deep inelastic reactions with a gold nucleus, the differing amounts of excitation energy, spin, etc., in the primary products that are derived from the gold nucleus, combine, after deexcitation, to produce a unique region of N and Z values. Since all the examples examined herein deal with deep inelastic collisions with gold, it would be interesting to see how these ''evaporation residue attractors'' change with reaction mechanism and target nuclei. The similarity between the data shown in Fig. 3, representing reactions of similar character but with otherwise measurably different outcomes, suggests an insensitivity of the fragment yield data to some features of the primary reaction mechanism.

The isobaric yield distribution obtained from integrating the independent yield distributions for each individual A value is shown in Fig. 5. The distribution is dominated by a broad central bump (thought to be due, in part, to fission) with lesser yields of the intermediate mass fragments ($A<60$) and the heavy residues ($A>150$). Integration of these distributions gives a cross sections of 3.3 b for ''fission'' ($A=60$–160, multiplicity 2) and 1.7 b for heavy residues ($A\geqslant 160$). It should be noted that this estimate of the ''fission'' cross section, while done in the manner typical of inclusive studies, may be in error. Bresson *et al.* [4], measured a fission cross section of 0.9–1.2 b for the fission of the Pb projectile in this reaction by direct detection of single fragments. While we are reporting a different quantity, the

TABLE I. Nuclide yields and recoil properties for the interaction of 29 MeV/nucleon ^{208}Pb with ^{197}Au.

Nucleus[a]	Cross section[b]	F/B	2W(F+B)[c]	Type of yield	Nuclide	Cross section[b]	F/B	2W(F+B)[c]	Type of yield
^{24}Na	20.9±2.8	71.3±9.1	33.8±4.6	*C*	^{103}Ru	20.1±0.6	9.6±0.2	24.1±0.4	*C*
^{28}Mg	11.0±0.9	107±5	37.7±2.3	*I*	^{105}Rh	19±12	6.5±4.3	18±11	*C*
^{38}S	5.3±2.3	93±40	34.3±0.6	*I*	^{105}Ru	6.6±1.1	6.9±0.1	27±2	*C*
^{42}K	27.6±3.5	85±10	33.8±2.5	*C*	^{105}Ag	18.5±2			*C*
^{43}K	26.8±8	82±23	36±11	*C*	^{106}Ag^{m}*	19.2±1.6			*I*
^{44}Sc	0.92±0.09			*C*	^{115}In^{m}*	8±5.4			*C*
^{44}Sc^{m}*	10.6±2.3			*I*	^{116}Te	7.8±6.2	14.7±4	13.3±7.9	*I*
^{46}Sc	27.7±5.9			*I*	^{119}Te	9.9±7.1			*C*
^{47}Ca	7.4±1.7			*I*	^{119}Te^{m}*	8.3±2.1			*I*
^{48}Sc	14.9±5.1	110/*pm* 37	33.7±4.5	*I*	^{120}I	15.2±2.3			*C*
^{48}V	4.2±1.1			*C*	^{121}Te	17.7±2.6			*C*
^{52}Mn	1.45±0.36			*C*	^{121}Te^{m}*	6.9±2.9			*C*
^{54}Mn	16.8±0.3			*I*	^{123}I	20±7.4	8.1±3	16.9±5.9	*C*
^{56}Mn	35.4±6.3	61±11	30.7±3.5	*C*	^{125}Xe	29.5±9.1	65±20	7.8±2.4	*C*
^{56}Co	2.4±1.3			*C*	^{127}Xe	27.9±2.7			*C*
^{59}Fe	25.6±5	26±5	30±2	*I*	^{131}Ba	23.7±2.4			*C*
^{65}Zn	18.6±1.9			*C*	^{132}Ce	12.1±1.2			*C*
^{65}Ni	7.4±1			*I*	^{132}Cs	1.5±0.2			*I*
^{69}Zn^{m}*	15.2±2	21.9±2.9	25.4±0.2	*I*	^{135} Ce	19.8±6.5			*C*
^{71}As	9.7±0.9			*C*	^{139}Ce	13±1.3			*C*
^{71}Zn^{m}*	2.9±2.3	14.5±2.5	25±10	*I*	^{145}Eu	16.2±6.3			*C*
^{72}As	9.4±1			*C*	^{147}Gd	12.1±1.3			*C*
^{72}Ga	13.4±8.3	20.5±8.6	25±10	*C*	^{147}Eu	20.8±2			*C*
^{73}Se	7.2±1.3	52±9	14.2±0.7	*C*	^{149}Gd	21.2±2.1			*C*
^{74}As	25.9±13.6	30.1±4.6	24.1±7.2	*I*	^{155}Dy	19.7±2			*C*
^{75}Se	26.1±5.7	26.4±5.3	26.4±4.5	*C*	^{157}Dy	14±1.7	63±7	9.6±0.4	*C*
^{76}As	17±2.7	15.8±1.9	19±1.2	*I*	^{169}Yb	21±6.4			*C*
^{76}Br	9.3±0.9			*C*	^{170}Hf	8.7±0.2			*C*
^{81}Rb	13.8±3.3	77±15	24±5.3	*C*	^{171}Hf	17.1±6.1			*C*
^{82}Br	7.5±1.2	11.9±0.3	24.2±1.9	*I*	^{171}Lu	23.2±2.6			*C*
^{83}Rb	41.5±9.7	26.5±1.7	21.7±2.8	*C*	^{173}Hf	19±0.6			*C*
^{83}Sr	12±2.4			*C*	^{173}Ta	10±1			*C*
^{84}Rb	24.2±2.4			*I*	^{175}Ta	22.8±7.4			*C*
^{85}Sr	33.9±1.1			*C*	^{175}Hf	21.9±2.2			*C*
^{87}Y	24.2±2.8			*C*	^{176}Ta	18.6±6			*C*
^{87}Y^{m}*	21±19	25±17	17±13	*C*	^{181}Re	27.2±1.8	66±4	4.7±0.3	*C*
^{88}Zr	18.8±2			*C*	^{183}Os^{m}*	15.2±1.6			*C*
^{89}Zr	23.2±3.9	52±7	20.7±3.1	*C*	^{183}Os	11.2±7.6			*C*
^{90}Y^{m}*	15.7±2.1	12.7±1	18.1±1.8	*I*	^{183}Re	41.3±4.5			*C*
^{92}Y	11.6±1.1			*C*	^{184}Ir	21.7±4.8			*C*
^{92}Sr	1.7±0.2	6.3±0.7	26.2±2.7	*I*	^{188}Pt	41.6±4.4			*C*
^{93}Mo^{m}*	13.3±1.4			*I*	^{191}Pt	52.2±6.6			*C*
^{94}Tc	7.6±1.6			*I*	^{192}Au	26.1±7.9	7.9±3.3	3.6±2.6	*C*
^{95}Zr	8.4±0.5	8.4±0.4	25.6±0.4	*C*	^{192}Hg	24.9±2.6			*C*
^{95}Tc	12.2±5.1			*C*	^{193}Hg^{m}*	35.7±9.1			*C*
^{95}Tc^{m}*	18.5±3.8			*C*	^{194}Au	93±20	8.2±1.7	3.1±0.6	*C*
^{96}Nb	18.3±6.1	9.9±2.7	20±3	*I*	^{195}Hg^{m}*	49.7±3.1			*I*
^{96}Tc	17.4±8			*I*	^{195}Au	156±35			*C*
^{97}Ru	10.8±0.5			*C*	^{196}Au	88.5±3.1	4.9±0.1	2.9±0.1	*C*
^{97}Zr	2.7±1	7.7±0.2	31±4	*I*	^{196}Au^{m}*	9.8±4.3	5.8±2.4	3.5±1.3	*I*
^{99}Mo	15.2±0.9	14.3±0.9	26.5±0.8	*C*	^{198}Au	29.6±3.1	10.8±0.4	3.1±0.3	*C*

[a]* denotes a nuclide not used in the computation of isobaric yields due to unknown yield of other members of isomeric pair.
[b]In mb.
[c]In mg/cm^2 Au.

TABLE II. Charge dispersion parameters for the reaction of 29 MeV/nucleon ^{208}Pb with ^{197}Au.

Mass number range	σ_A	a[a]	b[a]
24–59	0.6	0.365	0.442
65-76	0.8	0.365	0.442
81-90	0.9	0.201	0.442
92-106	1.1	1.93	0.419
115-120	1.0	2.16	0.419
121-127	0.6	5.11	0.394
131-139	0.9	9.75	0.359
145-157	0.6	10.4	0.359
169-176	0.5	11.8	0.350
181-188	0.6	-0.9	0.420
191-198	0.5	53.7	0.132

[a] $Z_{\rm mp} = aA + b$.

fission cross section for the gold target nucleus, we do not see a reason why it should exceed the fission cross section of the PLF by a factor of 3. Instead, we shall assert, based upon reaction simulations, and the fragment velocities, that portion of the cross section in this central bump may be due to lighter residues that resulted from the deexcitation of highly excited primary fragments. If we assume (see below) that 2.2 b is the fission cross section for the TLF, then the residue cross section is $1.7+(3.3-2.2)2=3.9$ b. The sum of these cross sections $(2.2+3.9=6.1)$ is less than the reaction cross section of 6.4 b [1], but ''missing'' events'' could easily be attributed to uncertainties in these estimates, inelastic events and multifragmentation events that leave no heavy residue.

However, we can better define our observations by noting that, besides the cross sections for various processes, we also have information about the recoil properties of the reaction products. To interpret these measured recoil properties in physically meaningful quantities, we have used mostly the integral catcher analysis method of Tobin and Karol [26]. In this analysis, we assume the final velocity of each fragment in the laboratory system can be written as $V_{\rm lab} = V + v$ where the velocity v is the velocity kick given to the fragment during the primary stage of the reaction and V is an average

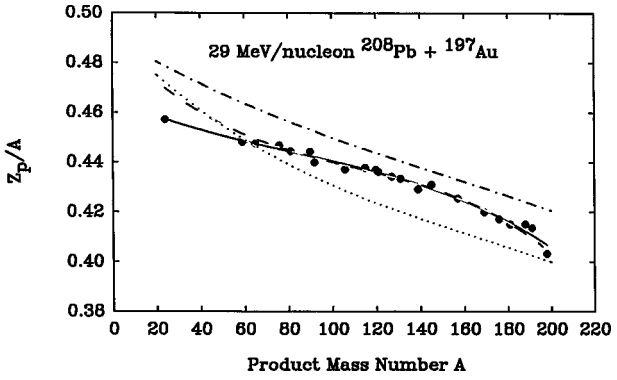

FIG. 2. Position of the most probable atomic number, Z_p, as a function of fragment mass number A. The dashed curve shows similar data for the 21 MeV /nucleon ^{129}Xe+^{197}Au reaction [28] while the dotted curve shows the line of beta stability and the dot-dashed line shows the Z_p values expected for relativistic nuclear collisions [23].

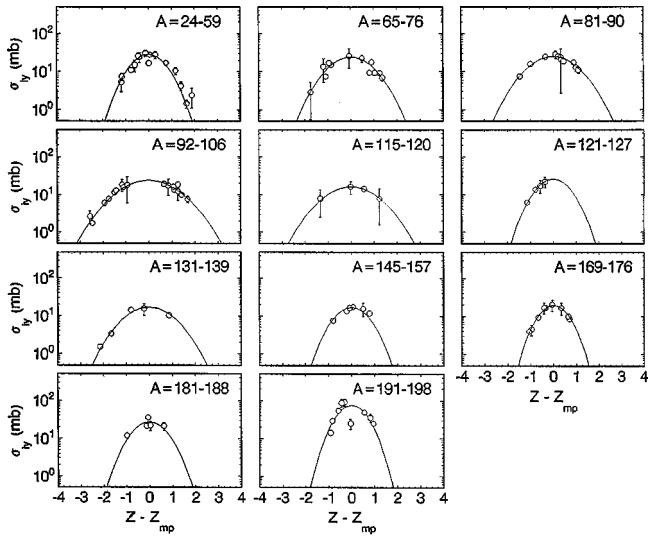

FIG. 3. The fragment independent yield distributions from the interaction of 29 MeV/nucleon ^{208}Pb with ^{197}Au. The plotted points are the independent yield cross sections calculated from the data while the solid lines are the Gaussian charge dispersions used in the calculation.

isotropic recoil velocity due to either sequential particle emission or fission. Since it is further assumed that $v = v_\parallel$, the average projection of the initial fragment velocity distribution on the beam axis, then V also includes an isotropic component of the velocity distribution in the initial stage of the reaction. (The case where there is a transverse velocity kick given in the initial stage of the reaction, is not considered, although values of $v_\perp = 0.25 v_\parallel$ have been shown [26] not to affect the analysis. Furthermore, Crespo, Alexander, and Hyde [27] have shown that due to canceling errors, the value of $v_\parallel$ is practically independent of $v_\perp / V$.) As opposed to a conventional analysis of recoil data, the Tobin-Karol method imposed no constraints on target thickness and corrected certain limitations and deficiencies in the conventional analysis.

The deduced values of v and V are shown in Figs. 6 and 7. The deduced longitudinal velocities are a small fraction of the complete fusion velocity (v_{CN}) and are slightly less than those observed in the 21 MeV/nucleon Xe + Au reaction.

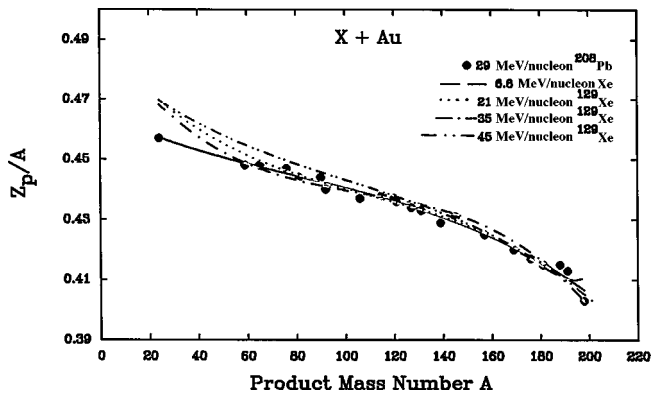

FIG. 4. The position of the most probable atomic number, Z_p, as a function of the fragment mass number A for a number of massive heavy ion-gold collisions [28,30].

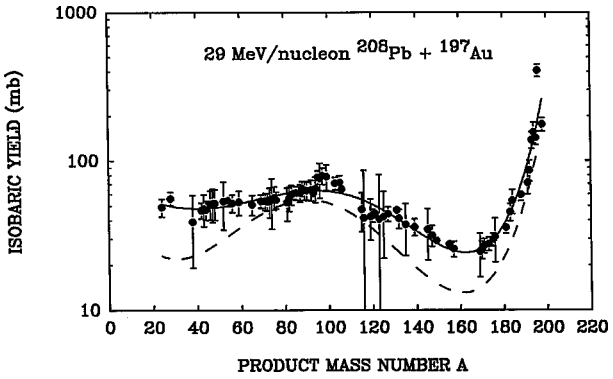

FIG. 5. Fragment isobaric yield distributions for the interaction of 29 MeV/nucleon ^{208}Pb with ^{197}Au.

This might be taken as an expected consequence of the increased preequilibrium emission (see below) for the reaction with the lead projectile relative to the xenon projectile.

The values of V, the velocity kick imparted to the products of the primary projectile-target interaction by fission or particle emission are compared to what one expects for the fission of a goldlike nucleus (Fig. 7). Some of the $A=40$–140 fragments have V values consistent with being the products of fission of a goldlike nucleus while there are other fragments with lower velocities. We will try to associate some of these fragments with lower values of V with a nonfission origin.

If we select the fragments with $60 \leqslant A \leqslant 140$, and plot the values of V versus the fragment N/Z ratio, we obtain Fig. 8. We see the higher values of V [that are consistent with a fissionlike process (Fig. 7)] are associated with the more neutron-rich fragments. The fragments of lower N/Z, presumably the result of extensive neutron emission, show lower values of V, consistent with a nonfission origin. If we note that a value of N/Z of about 1.3 corresponds to the expected velocities of the fission fragments, we can reintegrate the mass yield and charge distributions for this A range and $N/Z \geqslant 1.3$ to get a better estimate of the true fission cross section. This operation gives a value of 2.2 ± 0.5 b for the ''true'' fission cross section.

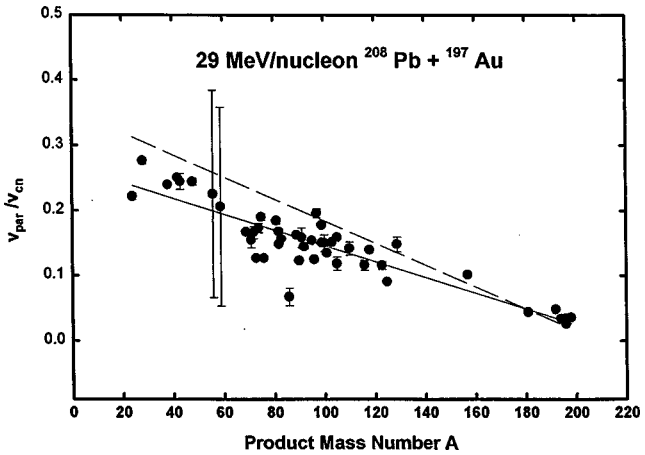

FIG. 6. Longitudinal fragment velocities (expressed as $v_{\parallel}/v_{CN}$) for the reaction studied in this work. The plotted points are the experimental data, the solid line represents a best fit to the data while the dashed line shows a best fit to similar data for the 21 MeV/nucleon ^{129}Xe+^{197}Au reaction.

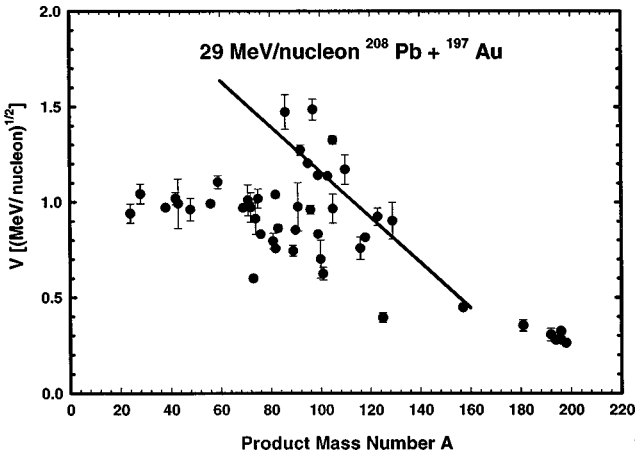

FIG. 7. The velocity V in the frame of the struck nucleus of the fragments from the interaction of 29 MeV/nucleon ^{208}Pb with ^{197}Au. The line represents the calculated fragment velocities assuming they resulted from the fission of ^{197}Au.

While our experiment is only indirectly sensitive to the angular momentum transfer, it can be noted that for ^{196}Au, the ratio of the independent yield of the high spin (12-) isomer to the low spin (2-) isomer is 0.11 ± 0.05. This is similar to the reaction of 21 MeV/nucleon ^{129}Xe with ^{197}Au, where the ''high spin/low spin'' ratio was 0.05. In the fission fragments, ^{87}Y, ^{119}Te and ^{121}Te, the ''high spin/low spin'' ratios (9/2 vs 1/2, 11/2 vs 1/2, 11/2 vs 1/2) are 0.9 ± 0.8, 1.1 ± 0.8, and 0.3 ± 0.2, respectively. For the intermediate mass fragment ^{44}Sc, this ratio (6+ vs 2+) was 11.5 ± 2.7. This data suggests that the angular momentum transfer in the events leading to residue production is modest, while the high angular momentum events decay by fission or preferentially by IMF emission.

A representative set of fragment angular distributions is shown in Fig. 9. The TLF angular distributions show a similar pattern to that observed for the reaction of 45 MeV/nucleon ^{129}Xe with ^{197}Au [31]. The distributions are sidewise peaked for fragments near the target mass number [$A=195$, due to quasielastic scattering, quarter point angle (lab) is 83°] to intermediate angle peaking ($A=149$–188)

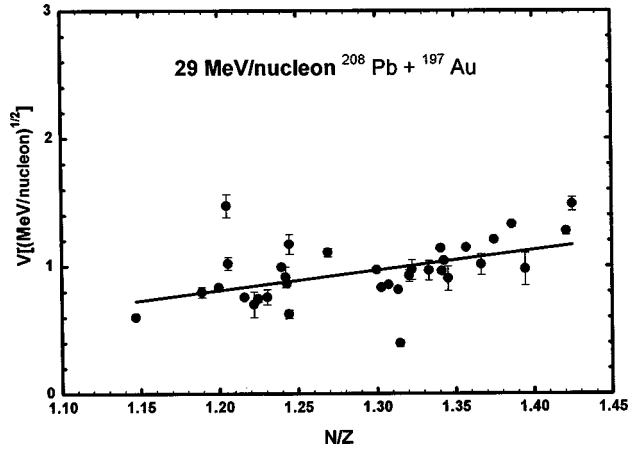

FIG. 8. The N/Z dependence of the fragment longitudinal momenta for fragments with $60 < A < 140$ from the interaction of 29 MeV/nucleon ^{208}Pb+^{197}Au. The solid line is a best fit to the data.

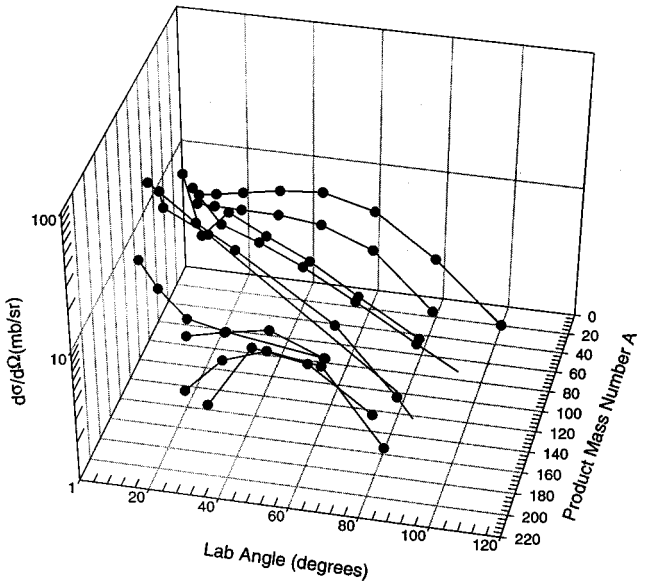

FIG. 9. Representative angular distributions of the fragments from the interaction of 29 MeV/nucleon ^{208}Pb with ^{197}Au.

to forward-peaked ($A<150$). This forward focusing of the TLF angular distributions with decreasing fragment mass is consistent with increasing momentum and energy transfer (Fig. 6).

It has been shown previously that the dominant reaction mechanism for the 29 MeV/nucleon ^{208}Pb+^{197}Au reaction involves binary dissipative collisions [3,5–7,11]. Further, it has been shown that the properties of the surviving residues of the primary projectile-like fragments (PLFs) result from the lowest multiplicity events that can be understood in terms of the nucleon exchange model [19] used to describe low energy deep inelastic scattering [2,6]. Given this background, we have used the nucleon exchange model to predict the primary TLF distributions for the Pb + Au reaction (Fig. 10) as a function of impact parameter. Since there is some indication in the literature [7,8,12,13] that there are difficulties with the predictions of the nucleon exchange model in describing PLF distributions, we have also modified the

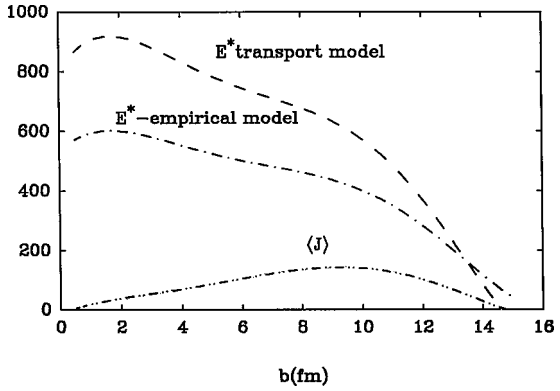

FIG. 10. The predictions of the nucleon transport model (and a modified version of it) for the characteristics of the primary TLFs. E^* and $\langle J\rangle$ refer to mean values of the excitation energy and angular momentum. The vertical scale can be used to read off both the energy in MeV or $\langle J\rangle$ in units of $\hbar$.

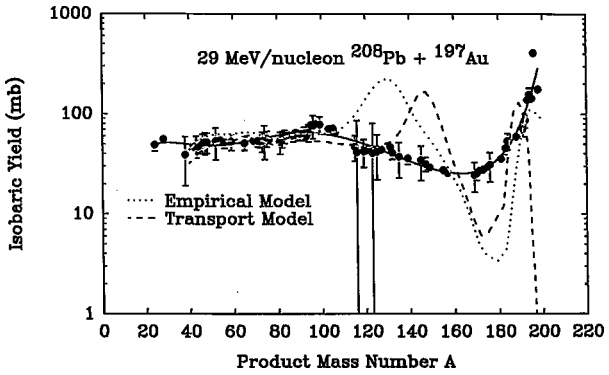

FIG. 11. Comparison of the predicted and measured values of the fragment mass distribution.

nucleon transport model predictions based upon the measurements and calculations [12] for the PLF distribution. These modifications lower the excitation energy and spin of the primary TLF to match direct observations of these quantities. These modified primary distributions are also shown in Fig. 10. The statistical model GEMINI [31] was used to model the deexcitation of the primary fragments. (Previous studies [11,12] have shown the suitability of this statistical model code for describing particle emission in this reaction.)

The resulting predictions of the nucleon transport model (''transport model'') and the empirically adjusted transport model (''empirical model'') are shown in Figs. 11 and 12. Both models predict a group of fragments with low excitation energies (quasielastic events) that roughly resemble the data in the magnitude of the cross section and their position in the N/Z plane. The bulk of the residues are predicted to have N/Z values that are similar to the observations ($A=60$–130) or are slightly more neutron-deficient than observed ($Z_{\rm pred}-Z_{\rm obs}$ 1.5 for $A=150$). Both simulations predict nonobserved peaks in the mass distribution. The magnitude of the ''nonobserved cross section'' in these peaks ($A=100$–160) is similar to that cross section that is ''missing'' from the near target cross sections. Detailed examination of the yield distributions associated with each impact parameter in the simulations shows these unusual peaks in the mass distribution result primarily from the more central collisions ($b<8$ fm) where the central density of the projectile and target nuclei overlap. One possibility is that it is these collisions that lead to multifragmentation which is not a part of

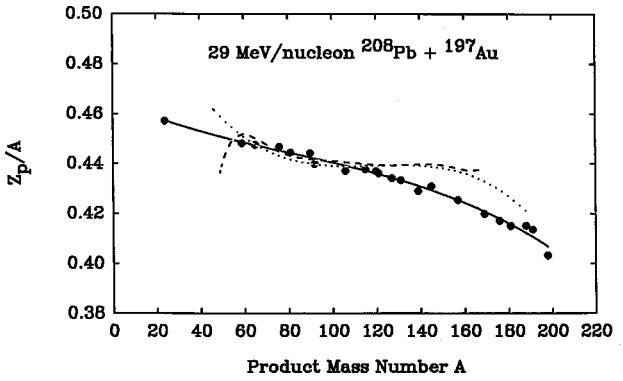

FIG. 12. Comparison of the predicted and measured values of the most probable fragment atomic numbers. The symbols have the same meaning as in Fig. 11.

these models of the dynamics of the initial projectile-target nuclear encounter. Further support for this idea is found in Fig. 10 where the predicted fragment excitation energies are shown to be similar to those expected for multifragmentation [9]. Thus it may not be surprising to see these discrepancies.

IV. CONCLUSIONS

What have we learned from this study of the production of heavy residues (targetlike fragments) in a collision of massive nuclei at intermediate energies?

(a) We have seen evidence (from the fragment velocities and N/Z ratios) that the heavy residue distribution can extend into the ''fission region,'' i.e., the large central bump in the fragment mass distributions. Simulations using the nucleon transport model predict (and perhaps overestimate) the occurrence of this phenomenon.

(b) The observed fragment mean N/Z values are relatively insensitive to the projectile energy in these collisions and as such, do not reflect the primary fragment distributions very much.

(c) The mean residue velocities (energies) are a small fraction of those observed in fusionlike collisions involving the interaction of lighter heavy ions with gold. The events leading to residue production involve low values of the transferred linear and angular momenta. (Higher l values are associated with fission and IMF emission.)

(d) The nucleon transport model which accounts for the basic features of these collisions also generally describes residue production (the fragment N/Z values) but fails to properly describe the outcomes on the more central ($b \leqslant 8$ fm) collisions.

ACKNOWLEDGMENTS

At GANIL, we appreciate the assistance of the operations and health physics staff who made these measurements possible. Three of us (N.H., D.M., and B.A.) acknowledge financial support from the NASA Space Grant Consortium at Oregon State University. One of us (J.V.) gratefully acknowledges support from the Institute of International Education. One of us (M.A.) wishes to acknowledge the support of the CHUST Committee of the Royal Institute of Technology in Stockholm. This work was supported in part by the U.S. Department of Energy under Grant DE-FG06-88ER40402 and the Swedish Natural Sciences Research Council.

[1] W.W. Wilcke, J.R. Birkelund, H.J. Wollersheim, A.D. Hoover, J.R. Huizenga, W.U. Schroder, and L.E. Tubbs, At. Data Nucl. Data Tables **26**, 391 (1984).
[2] E. Piasecki *et al.*, Phys. Rev. Lett. **66**, 1291 (1991).
[3] B.M. Quednau *et al.*, UR-NSRL-377, 1992.
[4] S. Bresson *et al.*, Phys. Lett. B **294**, 33 (1992).
[5] H.W. Barz, J.P. Bondorf, C.H. Dasso, R. Donangelo, G. Pollarolo, H. Schulz, and K. Sneppen, Phys. Rev. C **46**, R42 (1993).
[6] B.M. Quednau *et al.*, Phys. Lett. B **309**, 10 (1993).
[7] J.F. Lecolley *et al.*, Phys. Lett. B **325**, 317 (1994).
[8] J.F. Lecolley *et al.*, Phys. Lett. B **354**, 202 (1995).
[9] M. Aboufirassi *et al.*, LPCC-93-14, 1993.
[10] R. Bougault *et al.*, Nucl. Phys. **A587**, 499 (1995).
[11] M. Morjean *et al.*, Nucl. Phys. **A591**, 371 (1995).
[12] J. Colin *et al.*, Nucl. Phys. **A593**, 48 (1995).
[13] B. Jouault, V. de la Mota, F. Sebille, G. Royer, and J.F. Le Colley, Nucl. Phys. **A597**, 136 (1996).
[14] O. Granier *et al.*, Nucl. Phys. **A481**, 109 (1988).
[15] S.P. Baldwin *et al.*, UR-NSRL-29, 1993.
[16] S.P. Baldwin *et al.*, Phys. Rev. Lett. **74**, 1299 (1995).
[17] J. Toke *et al.*, Nucl. Phys. **A583**, 519 (1995).
[18] S.P. Baldwin, J. Toke, and W.U. Schroeder, DOE/ER/40414-7, 1994.
[19] J. Randrup, Nucl. Phys. **A307**, 319 (1978); **A327**, 490 (1979); **A383**, 468 (1982); J. Randrup and R. Vandenbosch, *ibid.* **A474**, 219 (1987); S.J. Luke, R. Vandenbosch, and J. Randrup, Phys. Rev. C **48**, 857 (1993).
[20] K. Aleklett *et al.*, Nucl. Phys. **A499**, 591 (1989).
[21] W. Loveland, K. Aleklett, J.O. Liljenzin, and G.T. Seaborg, J. Radioanal. Nucl. Chem. **160**, 181 (1992).
[22] F. Hubert, R. Bimbot, and H. Gauvin, At. Data Nucl. Data Tables **46**, 1 (1990).
[23] K. Sümmerer, W. Brüchle, D.J. Morrissey, M. Schadel, B. Szweryn, and Yang Weifan, Phys. Rev. C **42**, 2546 (1990).
[24] R.J. Charity, Phys. Rev. C **58**, 1073 (1998).
[25] D.J. Morrissey, W. Loveland, M. de Saint-Simon, and G.T. Seaborg, Phys. Rev. C **21**, 1783 (1980).
[26] M.J. Tobin and P.J. Karol, Nucl. Instrum. Methods Phys. Res. A **270**, 511 (1988).
[27] V.P. Crespo, J.M. Alexander, and E. Hyde, Phys. Rev. **131**, 1765 (1963).
[28] A. Yokoyama, W. Loveland, J.O. Liljenzin, K. Aleklett, D.J. Morrissey, and G.T. Seaborg, Phys. Rev. C **46**, 647 (1992).
[29] J.V. Kratz, J. Poitou, W. Bruchle, H. Gaggeler, M. Schadel, G. Wirth, and R. Lucas, Nucl. Phys. **A357**, 437 (1981).
[30] W. Loveland, K. Aleklett, R. Yanez, A. Srivastava, and J.O. Liljenzin, Phys. Lett. B **312**, 53 (1993).
[31] R.J. Charity *et al.*, Nucl. Phys. **A483**, 371 (1988).